Dyes and Pigments 106 (2014) 58–70

Contents lists available at ScienceDirect

Dyes and Pigments

journal homepage: www.elsevier.com/locate/dyepig

New derivatives of triphenylamine and naphthalimide as ambipolar organic semiconductors: Experimental and theoretical approach

Dalius Gudeika [a], Juozas Vidas Grazulevicius [a,*], Gjergji Sini [b,**], Audrius Bucinskas [a], Vygintas Jankauskas [c], Arunas Miasojedovas [d], Saulius Jursenas [d]

[a] Department of Polymer Chemistry and Technology, Kaunas University of Technology, Radvilenu pl. 19, LT-50254 Kaunas, Lithuania
[b] Laboratoire de Physicochimie des Polymères et des Interfaces, EA 2528 Université de Cergy-Pontoise, 5 mail Gay-Lussac, 95031 Cergy-Pontoise Cedex, France
[c] Department of Solid State Electronics, Vilnius University, Sauletekio aleja 9, LT-10222 Vilnius, Lithuania
[d] Institute of Applied Research, Vilnius University, Sauletekio aleja 9, LT-10222 Vilnius, Lithuania

ARTICLE INFO

Article history:
Received 30 December 2013
Received in revised form
21 February 2014
Accepted 25 February 2014
Available online 6 March 2014

Keywords:
Donor–acceptor
Suzuki condensation
Triphenylamine
1,8-Naphthalimide
DFT
Ambipolar charge transfer

ABSTRACT

Four new derivatives of triphenylamine containing different number of naphthalimide moieties were designed and synthesized by Suzuki condensation and their properties were studied by the experimental and theoretical tools. The compounds obtained are capable to form molecular glasses with glass transition temperatures ranging from 45 °C to 84 °C. They exhibit very high thermal stabilities with 5% weight loss temperatures ranging from 429 °C to 483 °C. Fluorescence quantum yields of the dilute solutions in nonpolar solvents of the synthesized materials range from 0.63 to 0.78. Due to the pronounced electron donor–acceptor character, the compounds show dramatic solvatochromic red shifts of fluorescence (up to 250 nm) in polar solvents. The ionization potentials of the solid samples of the compounds established by electron photoemission spectrometry in air ranged from 5.57 to 6.01 eV. 4-(4′-(Di-(4″-methoxyphenyl)amino)phenyl)-*N*-(2-ethylhexyl)-1,8-naphthalimide (**5**) was found to show ambipolar charge transport in air with the mobilities of charges exceeding 10^{-4} cm^2 V^{-1} s^{-1} at high electric fields. The electron mobility of the compounds containing no methoxy groups were found to exceed the hole mobility by 2–3 orders of magnitude. The special role of methoxy groups in the ambipolar charge transport character of compound **5** is discussed in the frame of hopping Marcus theory, by applying a static theoretical analysis followed by a qualitative discussion of the positional disorder in some of these materials.

1. Introduction

In the last decades many kinds of organic hole-transporting amorphous molecular materials were reported [1]. Lesser assortment is available of glass-forming electron-transporting organic molecular materials especially those capable of working in air [2,3]. Even smaller amount of amorphous organic molecular materials capable of effectively transporting both holes and electrons were reported, however such materials recently attract much attention [4,5]. Ambipolar charge-transporting materials are of interest for applications in organic light emitting diodes (OLED) [6] and in particular in electrophosphorescent devices [7a]. In the continual effort to search for ideal materials for OLEDs, small molecules with ambipolar charge transporting character are extremely attractive as they offer the possibility to achieve efficient and stable OLEDs even in a simple single-layer configuration. Organic ambipolar semiconductors are divided into two categories [4]. One category is represented by materials the molecules of which consist both of donor and acceptor moieties. Such materials are widely studied as dyes for dye sensitized solar cells [7b]. The materials composed of the molecules having no donor–acceptor structure are assigned to another category. The molecules of the latter category usually have extended systems of conjugated π-electrons. Most of the ambipolar organic semiconductors are capable of transporting both holes and electrons when protected from air. Much less information is reported on the materials capable of transporting both negative and positive charges at ambient conditions [8,9].

* Corresponding author. Tel.: +370 37 300193; fax: +370 37 300152.
** Corresponding author.
E-mail addresses: juozas.grazulevicius@ktu.lt (J.V. Grazulevicius), gjergji.sini@u-cergy.fr (G. Sini).

http://dx.doi.org/10.1016/j.dyepig.2014.02.023
0143-7208/

In this article we report on the synthesis and properties of organic semiconductors consisting of 1,8-naphthalimide and triphenylamine (TPA) moieties capable of effectively transporting both holes and electrons in air. 1,8-Naphthalimide derivatives represent an interesting group of electron-deficient organic materials with promising electron-transporting properties [10]. Electron-rich TPA derivatives have been typically used as hole-transporting materials and/or blue light emitting materials [11] due to the easy oxidizability of the nitrogen centre and the ability to transport positive charges via the radical-cation species. These properties are related to the presence of nitrogen atom linked to three electron rich phenyl groups in a three-dimensional propeller-like shape [12]. The photoinduced electron transfer was recently observed in the solutions of the derivatives of 1,8-naphthalimide and TPA [13]. Hydrazones containing 1,8-naphthalimide and triphenylamino moieties were found to be capable of transporting only positive charges in air [14]. To our knowledge no studies demonstrating ambipolar charge transport in the derivatives of 1,8-naphthalimide and TPA were yet reported.

The role of different substituents on the ionization potentials and other parameters of TPA-based compounds has been already considered [15–18]. It is well established that methoxy groups decrease the ionization potentials of the TPA-based compounds [15,16], influencing consequently the hole-injection barrier in the devices. However, lower charge mobility was recorded for instance in the case of *p*-methoxy and *p*-buthoxy substituted *N*,*N*′-bis(*m*-tolyl)-*N*,*N*′-diphenyl-1,1′-biphenyl-4,4′-diamine (TPD) as compared to the non-substituted TPD, which was in part explained by the role of the disorder on the dipole moments of these molecules [17]. Interestingly, the hole transporting properties of TPA-based compounds were recently found to be enhanced by the presence of methoxy groups in para-positions of the phenyl moieties [19], which was partly explained by the hydrogen-bonding capacity of the methoxy groups. As it will be shown in the following, among the newly synthesized compounds, the ambipolar charge transport properties of one of them containing methoxy groups are superior, as compared to the compounds containing no methoxy groups. It is consequently very intriguing to understand the reasons for the higher electron-versus hole mobilities on the one hand, and for the higher hole mobility of the methoxy-substituted compound (by three orders of magnitude) as compared to the non-substituted ones.

By applying a joint experimental and theoretical approaches, the aim of this study is twofold: (i) report on the synthesis of four new derivatives of TPA containing direct linkages with a different number of naphthalimide moieties (ii) characterization of the four new compounds for better understanding of the structure–property relationships. The hole-transport properties of these amorphous compounds are discussed in the frame of Marcus theory [20–23].

2. Experimental

2.1. Synthesis

Materials. 4-Bromo-1,8-naphtalic anhydride, 4-bromoaniline and 2-ethylhexylamine purchased from TCI, TPA, 1-iodo-4-methoxybenzene, tris(4-bromophenyl)amine, 4-(diphenylamino)phenylboronic acid, *n*-BuLi (2.5 mol L^{-1} in hexane), 2-isopropoxy-4,4,5,5-tetramethyl-1,3,2-dioxaborolane, bis(triphenylphosphine)palladium(II) dichloride ($Pd(PPh_3)_2Cl_2$), *N*-bromosuccinimide (NBS) and 1,10-phenanthroline purchased from Aldrich were used as received. Dimethylformamide (DMF, Lachema) was dried by distillation over CaH_2. THF was dried and distilled over sodium and benzophenone. Dichloromethane (POCH), ethyl acetate and *n*-hexane (Penta) were purified and dried using the standard procedures [24]. 4-Bromo-*N*-(2-ethylhexyl)-1,8-naphthalimide (**1**) [14], (4-bromo-phenyl)-di-(4-methoxyphenyl)-amine (**2b**) [25], bis(4-bromophenyl)phenylamine (**2c**) [26], bis(4-(4,4,5,5-tetramethyl-(1,3,2)dioxaborolan-2-yl)-phenyl)phenylamine (**3c**) [27], 4-(4,4,5,5-tetramethyl-(1,3,2)dioxaborolan-2-yl)-phenyl)-di-(4-methoxyphenyl)-amine (**3b**) [28], tris(4-(4,4,5,5-tetramethyl-(1,3,2)dioxaborolan-2-yl)-phenyl)phenylamine (**3d**) [29] were prepared according to the published procedures.

2.1.1. 4-(4′-Diphenylaminophenyl)-N-ethylhexyl-1,8-naphthalimide (4)

The solution of 4-bromo-1,8-naphthalimide (**1**) (0.5 g, 1.29 mmol) and $Pd(PPh_3)_2Cl_2$ (0.03 g, 0.04 mmol) in THF (15 mL) was purged with nitrogen, and the solution of 4-(diphenylamino) phenylboronic acid (0.37 g, 1.28 mmol) in THF (3 mL) and aqueous K_2CO_3 solution (1.70 g, 12.32 mmol) in H_2O (2 mL) were added with a syringe. The reaction mixture was stirred at 80 °C for 24 h. After cooling down, the product was extracted with CH_2Cl_2, washed with water and dried over $MgSO_4$. The solvent was evaporated to afford a crude product. After column chromatography on silica gel with the eluent mixture of ethyl acetate and hexane (1:8, V:V), compound **4** was obtained as yellow powder with the yield of 0.55 g (78%). M.p. 127–128 °C; R_f = 0.54; ^{1}H NMR (300 MHz, $CDCl_3$): δ 8.67 (d, 1H, J = 7.32 Hz, $H_{Naphthalene}$), 8.66 (d, 1H, J = 8.52 Hz, $H_{Naphthalene}$), 8.46 (d, 1H, J = 1.16 Hz, $H_{Naphthalene}$), 8.43 (d, 1H, J = 1.15 Hz, $H_{Naphthalene}$), 7.75 (t, 1H, J = 7.56 Hz, $H_{Naphthalene}$), 7.44–7.31 (m, 6H, –Ar), 7.27–7.09 (m, 8H, –Ar), 4.26–4.11 (m, 2H, $-CH_2$, $-H_{aliphatic}$), 2.06–1.95 (m, 1H, –CH, $-H_{aliphatic}$), 1.48–1.31 (m, 8H, 4 × CH_2, $-H_{aliphatic}$), 1.01–0.89 (m, 6H, 2 × CH_3, $-H_{aliphatic}$). ^{13}C NMR (75.4 MHz, $CDCl_3$): δ 167.43, 147.76, 146.75, 146.14, 132.85, 131.90, 131.48, 131.29, 130.31, 130.05, 129.31, 128.42, 127.93, 126.73, 125.78, 124.77, 123.83, 121.64, 43.87, 38.14, 31.73, 28.88, 24.59, 23.47, 14.44, 10.82. IR (KBr, υ cm^{-1}): 3060 (CH_{ar}), 2954, 2925, 2858 ($CH_{aliphatic}$), 1697 ($C{=}O_{anhydride}$), 1656, 1584, 1505, 1486 ($C{=}C_{ar}$), 1350, 1279 (C–N), 784, 759, 695 (CH_{ar}); Anal. Calcd. for $C_{38}H_{36}N_2O_2$: C, 82.58; H, 6.57; N, 5.07; O, 5.79. Found: C, 82.63; H, 6.60; N, 5.08. MS (APCI$^+$, 20 V), *m*/*z*: 553 ($[M + H]^+$)

2.1.2. 4-(4′-(Di-(4″-methoxyphenyl)amino)phenyl)-N-(2-ethylhexyl)-1,8-naphthalimide (5)

4-(4′-(Di-(4″-methoxyphenyl)amino)phenyl)-*N*-(2-ethylhexyl)-1,8-naphthalimide **(5)** was prepared by the similar procedure as **4** using **3b** (0.58 g, 1.42 mmol), **1** (0.5 g, 1.29 mmol), $Pd(PPh_3)_2Cl_2$ (0.03 g, 0.039 mmol), K_2CO_3 (1.78 g, 12.89 mmol). The crude product was purified by silica gel column chromatography using the mixture of ethyl acetate and hexane (1:8, V:V) as an eluent to obtain **5** as amorphous material with the yield of 0.59 g (75%); R_f = 0.51; ^{1}H NMR (300 MHz, $CDCl_3$): δ 8.66 (d, 1H, J = 7.37 Hz, $H_{Naphthalene}$), 8.64 (d, 1H, J = 7.44 Hz, $H_{Naphthalene}$), 8.45 (d, 1H, J = 1.14 Hz, $H_{Naphthalene}$), 7.73 (t, 2H, J = 8.19 Hz, $H_{Naphthalene}$), 7.35 (d, 2H, J = 8.81 Hz, –Ar), 7.20 (d, 4H, J = 9.05 Hz, –Ar), 7.08 (d, 2H, J = 8.78 Hz, –Ar), 6.92 (d, 4H, J = 9.05 Hz, –Ar), 4.24–4.12 (m, 2H, $-CH_2$, $-H_{aliphatic}$), 3.85 (s, 6H, 2 × OCH_3), 2.04–1.94 (m, 1H, –CH, $-H_{aliphatic}$), 1.48–1.30 (m, 8H, 4 × CH_2, $-H_{aliphatic}$), 1.01–0.90 (m, 6H, 2 × CH_3, $-H_{aliphatic}$). ^{13}C NMR (75.4 MHz, $CDCl_3$): δ 164.95, 156.78, 149.49, 147.29, 140.44, 133.20, 131.33, 130.87, 130.09, 127.87, 127.71, 127.32, 126.84, 123.12, 121.28, 119.63, 115.12, 55.72, 44.33, 38.15, 30.97, 28.96, 24.38, 23.33, 14.36, 10.89. IR (KBr, υ cm^{-1}): 3037 (CH_{ar}), 2955, 2927, 2856 ($CH_{aliphatic}$), 1698 ($C{=}O_{anhydride}$), 1657, 1586, 1504, 1463 ($C{=}C_{ar}$), 1440, 1425 (OCH_3), 1354, 1282 (C–N), 784, 758, 656 (CH_{ar}). Anal. Calcd. for $C_{40}H_{40}N_2O_4$: C, 78.40; H, 6.58; N, 4.57; O, 10.44. Found: C, 78.45; H, 6.65; N, 4.52. MS (APCI$^+$, 20 V), *m*/*z*: 613 ($[M + H]^+$)

2.1.3. 4,4′-(Di(N-(2-ethylhexyl)-1,8-naphthalimide-4-yl)phenyl) benzenamine (6)

4,4′-(Di(*N*-(2-ethylhexyl)-1,8-naphthalimide-4-yl)phenyl)benzenamine **(6)** was prepared by the similar procedure as **4** using **3c** (0.28 g, 0.59 mmol), **1** (0.5 g, 1.29 mmol), $(PPh_3)_2Cl_2$ (0.02 g, 0.035 mmol), K_2CO_3 (1.21 g, 8.79 mmol). The crude product was purified by silica gel column chromatography using the mixture of ethyl acetate and hexane (1:8, V:V) as an eluent to obtain 6 as a red crystals with the yield of 0.32 g (64%). M.p. 131–132 °C; $R_f = 0.48$; ^{1}H NMR (300 MHz, $CDCl_3$): δ 8.68 (d, 4H, $J = 7.52$ Hz, $H_{Naphthalene}$), 8.46 (d, 2H, $J = 8.48$ Hz, $H_{Naphthalene}$), 7.84–7.71 (m, 4H, $H_{Naphthalene}$), 7.56–7.34 (m, 11H, –Ar), 7.27–7.20 (m, 1H, –Ar), 4.25–4.12 (m, 4H, 2 × CH_2, $-H_{aliphatic}$), 2.05–1.97 (m, 2H, 2 × CH, $-H_{aliphatic}$), 1.53–1.29 (m, 16H, 8 × CH_2, $-H_{aliphatic}$), 1.06–0.85 (m, 12H, 4 × CH_3, $-H_{aliphatic}$). ^{13}C NMR (75.4 MHz, $CDCl_3$): δ 164.79, 148.09, 147.24, 146.63, 133.27, 132.82, 131.50, 131.27, 130.24, 130.02, 129.08, 128.02, 127.02, 126.01, 124.57, 123.80, 123.28, 121.78, 44.45, 38.23, 31.05, 29.00, 24.35, 23.37, 14.39, 10.96. IR (KBr, υ cm^{-1}): 3032 (CH_{ar}), 2955, 2926, 2856 ($CH_{aliphatic}$), 1701 ($C{=}O_{anhydride}$), 1659, 1587, 1504, 1464 ($C{=}C_{ar}$), 1353, 1284 (C–N), 783, 758, 697 (CH_{ar}). Anal. Calcd. for $C_{58}H_{57}N_3O_4$: C, 80.99; H, 6.68; N, 4.89; O, 7.44. Found: C, 81.06; H, 6.65; N, 4.92. MS (APCI$^+$, 20 V), *m*/*z*: 861 ($[M + H]^+$)

2.1.4. 4,4′,4‴-(Tris(N-(2-ethylhexyl)-1,8-naphthalimide-4-yl) phenyl)benzenamine (7)

4,4′,4‴-(Tris(N-(2-ethylhexyl)-1,8-naphthalimide-4-yl)phenyl) benzenamine **(7)** was prepared by the similar procedure as **4** using **3d** (0.23 g, 0.39 mmol), **1** (0.5 g, 1.29 mmol), $(PPh_3)_2Cl_2$ (0.02 g, 0.035 mmol), K_2CO_3 (1.08 g, 7.81 mmol). The crude product was purified by silica gel column chromatography using the eluent mixture of ethyl acetate and hexane (1:8, V:V) to obtain 7 as a yellow crystals with the yield of 0.15 g (34%). M.p. 133–134 °C; $R_f = 0.36$; ^{1}H NMR (300 MHz, $CDCl_3$): δ 8.71 (d, 3H, $J = 2.76$ Hz, $H_{Naphthalene}$), 8.69 (d, 3H, $J = 2.51$ Hz, $H_{Naphthalene}$), 8.47 (d, 3H, $J_1 = 8.64$ Hz, $H_{Naphthalene}$), 7.76 (t, 6H, $J = 7.70$ Hz, $H_{Naphthalene}$), 7.58 (d, 6H, $J = 8.68$ Hz, –Ar), 7.51 (d, 6H, $J = 8.69$ Hz, –Ar), 4.26-4.12 (m, 6H, 3 × CH_2, $-H_{aliphatic}$), 2.04–1.96 (m, 3H, 3 × CH, $-H_{aliphatic}$), 1.48–1.32 (m, 24H, 12 × CH_2, $-H_{aliphatic}$), 1.00–0.91 (m, 18H, 6 × CH_3, $-H_{aliphatic}$). ^{13}C NMR (75.4 MHz, $CDCl_3$): δ 162.58, 145.32, 146.44, 133.32, 133.87, 132.56, 132.24, 129.76, 129.11, 127.88, 127.14, 125.98, 125.12, 123.78, 123.27, 121.88, 44.47, 38.33, 31.15, 28.95, 24.23, 23.27, 14.32, 11.03. IR (KBr, υ cm^{-1}): (CH_{ar}), 2956, 2927, 2857 ($CH_{aliphatic}$), 1700 ($C{=}O_{anhydride}$), 1659, 1586, 1504, 1464 ($C{=}C_{ar}$), 1354, 1281 (C–N), 783, 758, 696 (CH_{ar}). Anal. Calcd. for $C_{78}H_{78}N_4O_6$: C, 80.24; H, 6.73; N, 4.80; O, 8.22. Found: C, 80.29; H, 6.79; N, 4.85. MS (APCI$^+$, 20 V), *m*/*z*: 1168 ($[M + H]^+$).

2.2. Computational details

The theoretical study was carried out in the frame of density functional theory (DFT) [30] employing the B3LYP [31] functional in conjunction with the 6-31G(d,p) basis set. The geometry optimizations of the model compounds **M4**–**M7** (containing methyl substituents instead of the experimental ones) were performed in absence of medium effects without symmetry constraints. All the geometry optimizations were followed by frequency calculations in order to verify if real minima were obtained. The geometry optimizations of the cationic radical species were performed at the unrestricted open shell level.

The spectroscopic properties of the molecules were analysed in the frame of time dependent density functional theory method (TDDFT) [32]. The theoretical absorption bands were obtained by considering a band half-width of 0.2 eV at half-height (Gaussview 5 software).

The vertical ionization potentials (I_p) were calculated at the B3LYP/6-31G(d,p) level as energy difference between neutral and radical cation species at the neutral state geometry (optimized geometries for the adiabatic I_p).

The internal reorganization energy (λ_i) values of model compounds **M4**–**M7** were calculated at the B3LYP/6-31G(d,p) level according to the following equation [33]:

$$\lambda_l = \lambda_l^1 + \lambda_l^2 = \left(E_M^{Geom(M^+)} - E_M^{Geom(M)}\right) + \left(E_{M^+}^{Geom(M)} - E_{M^+}^{Geom(M^+)}\right)$$

In this equation, the quantity E_M for instance corresponds to the energy of the neutral molecule (M) in the geometry of the cationic species (M^+).

The geometries of some selected dimers formed by two identical **M4** and **M5** molecules have been optimized by employing the wB97X-D [34] functional at the 6-31G(d,p) basis set. Previous studies have shown that this functional provides good results on the description of weak interactions [35,36]. The solvent effect (tetrahydrofuran in this case) was also taken into account during the dimer geometry-optimizations by using the conductor-like polarizable continuum model (CPCM) [37]. The electronic couplings between the HOMO orbitals of two adjacent molecules were calculated at the B3LYP/6-31G(d,p) level, according to the approach described by Valeev et al. [38] with the corresponding matrix elements evaluated with Gaussian 09 [39]. Note that the coupling values depend on the functional used and generally increase with the increasing percentage of Hartree–Fock exchange in the functional [35]. The transfer integrals calculated by using two different functionals are thus expected to change roughly by a constant factor, but the trends obtained for both functionals should be the same.

The interaction free energies of some optimized dimers were calculated with respect to the isolated monomers at the wB97XD/6-31G(d,p) level and were corrected for the basis set superposition error (BSSE) by using the counterpoise correction method of Boys and Bernardi [40].

3. Results and discussions

3.1. Synthesis and characterization

Scheme 1 shows the synthetic routes to compounds **4**–**7**. The first step was condensation of 4-bromo-1,8-naphtalic anhydride (**BRA**) with 2-ethylhexylamine in DMF which gave 4-bromo-*N*-(2-ethylhexyl)-1,8-naphthalimide (**1**). Compound **2b** was obtained by Ullmann coupling of 4-bromoaniline (**1b**) with 1-iodo-4-methoxybenzene [41]. Compound **2c** was prepared by bromination of TPA (**1c**) with *N*-bromosuccinimide. Compounds **3b-d** were obtained by the reactions of **2b, 2c** and commercially available tris(4-bromophenyl)amine (**2d**) with *n*-BuLi at −78 °C and the following quenching with 2-isopropoxy-4,4,5,5-tetramethyl-1,3,2-dioxaborolane. 4-(4′-Diphenylaminophenyl)-*N*-ethylhexyl-1,8-naphthalimide (**4**) was synthesized by Suzuki coupling of 4-bromo-*N*-(2-ethylhexyl)-1,8-naphthalimide (**1**) with 4-(diphenylamino)phenylboronic acid (**3a**). Compounds **5**–**7**, were also synthesized by the Suzuki coupling reactions between compounds **3b-d** and compound **1** under nitrogen atmosphere. All the derivatives were characterized by ^{1}H and ^{13}C NMR, mass spectrometries and elemental analysis.

The target compounds (**4**–**7**) are soluble in common organic solvents such as dichloromethane (DCM), chloroform, tetrahydrofuran (THF), chlorobenzene and toluene.

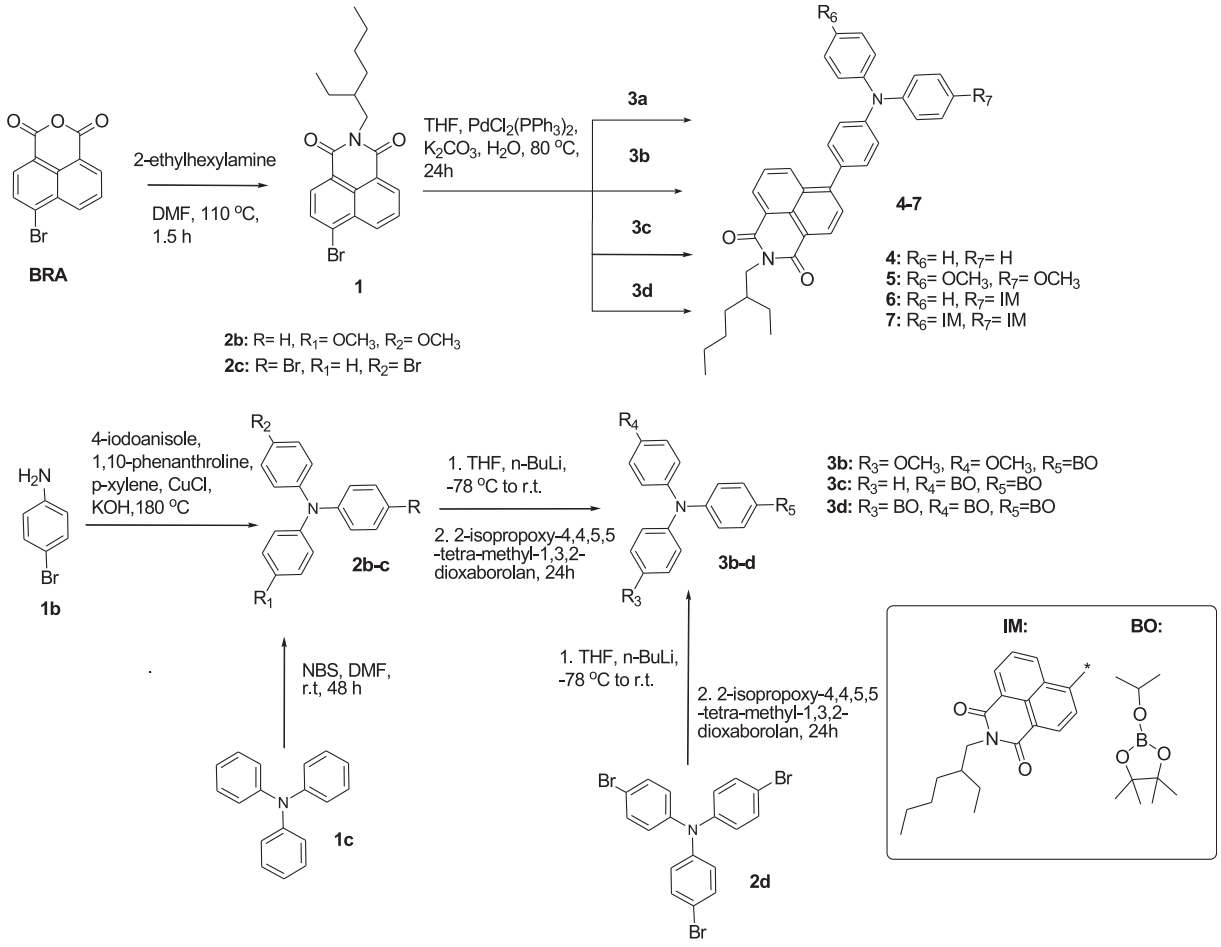

Scheme 1. The synthetic routes to **4**–**7**.

3.2. Geometries and frontier orbitals

The geometries of model compounds **M4**–**M7**, (containing methyl groups instead of the experimental alkyl groups) are presented in Fig. 1, along with some relevant geometrical parameters.

The TPA N atom of each compound and the three appended carbon atoms form a plane (reported hereafter as "N-plane"), due to the π-conjugation between the phenyl groups and the lone pair of the central N atom. In the case of **M5**, only one conformer is presented. Other conformers of similar energy can be assumed, with the methoxy groups combined in different orientations. Compared to the model compound **M4**, the geometry around the N(TPA) atom in **M5** has more quinoidal character, which is due to the π-donor effect of the methoxy groups. The same observation can be done when comparing **M5** with **M6** and **M7**. The frontier orbitals for the three molecules are given in Fig. 2.

3.3. Thermal properties

The thermal properties of **4**–**7** were examined by DSC and TGA under a nitrogen atmosphere. The values of glass transition temperatures (T_g), melting points (T_m) and 5% weight loss temperatures (T_{ID}) are summarized in Table 1. TGA revealed that all the target compounds exhibit excellent thermal stabilities. Their T_{ID} range from 429 to 483 °C. These temperatures are close to 5% weight loss temperatures of methoxy-substituted derivatives of TPA [19]. Increase of the number of 1,8-naphthalimide moieties leads to the increase of the thermal stability of the derivatives. Molecules **6, 7** having two and three 1,8-naphthalimide moieties showed higher 5% weight loss temperatures than molecules **4** and **5** containing one 1,8-naphthalimide moiety.

Compounds **4**, **6** and **7** were obtained as crystalline materials. Their first DSC heating scans revealed melting in the range of 134–148 °C. Their second DSC heating scans revealed the glass transitions in the range of 45–93 °C and no peaks due to crystallization appeared. The values of T_g of molecular glasses of **4**–**7** are affected by the number of naphthalimido moieties in the *para* positions of triphenylamino moiety and increase in the order **4** < **6** < **7**. The lower T_g values of **4** and **5** can apparently be explained in terms of their lower molecular weight and lower intermolecular interaction. The DSC traces of **5** did not display transition associated with melting even during repeated scans. The absence of melting confirms the amorphous character of **5**. This observation can apparently be attributed to the presence of methoxy groups at the triphenylamino moiety which increase the disorder in the molecule packing. Previously it has been suggested that C–H...π short contacts can be established between the methoxy groups and the phenyl groups [19]. C–H…π short contacts of different interaction energies may thus be present in the films of compound **5**, which might be responsible for the absence of a well-defined melting temperature. The amorphous nature of compound **5** is also reflected in its enhanced solubility. Fig. 3 shows DSC thermograms of compound **4**. During the first heating scan of the sample of **4** endothermal melting signal at 134 °C was observed. After re-

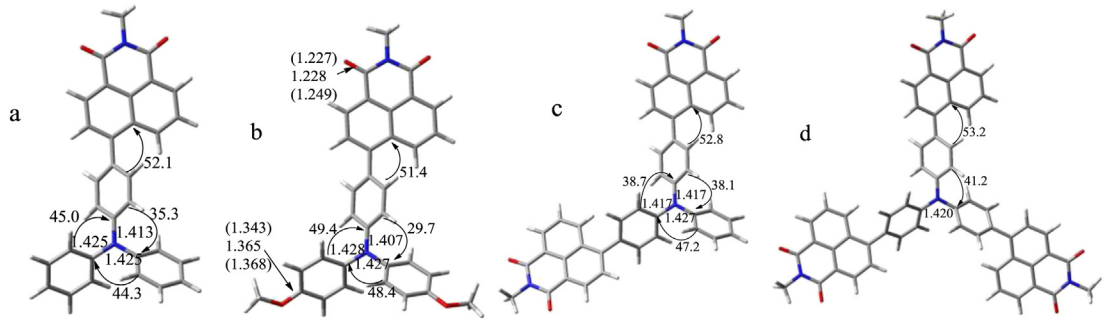

Fig. 1. Optimized geometries of M4 (a), M5 (b), M6 (c), and M7 (d) model compounds, obtained at the B3LYP/6-31G(d,p) level. Some relevant bond-lengths (N–C bondlengths in TPA core in Å) and dihedral angles (absolute values in degrees) are shown. The C–O bond-lengths for compound M5 in the neutral state are also indicated, along with the same distances in the cationic and anionic states (shorter and longer distances respectively in parentheses).

cooling, the following second heating scan revealed glass transition at 47 °C and no crystallization signal was observed. This observation shows that the material can exist in solid amorphous state and can be considered as molecular glass.

3.4. Optical and photophysical properties

UV–VIS absorption spectra and fluorescence spectra of dilute solutions in nonpolar cyclohexane, of dilute solid solutions in polystyrene (PS) matrixes, and of neat films of the investigated TPA and naphthalimide derivatives are shown in Fig. 4 (see also Fig. S1 in the Supporting Information (SI)). The photophysical characteristics of the compounds are summarized in Table 2.

The theoretical UV–VIS spectra for the model compounds **M4**–**M7** (Fig. S2 (SI)) suggest that the absorption bands peaking at about 320 nm and 350 nm (Fig. 4) correspond to local π-π* electron transitions of the triphenylamino moieties and naphthalimide fragments [42], respectively. Absorption peaks which appear in the range of 406–436 nm correspond to HOMO → LUMO electronic transition, with HOMO and LUMO orbitals being almost exclusively localized on the donor and acceptor moieties, respectively (Fig. 2). These broad unstructured bands correspond consequently to the intramolecular charge-transfer transitions between the TPA donor moieties and the naphthalimide acceptor moieties. In the case of compounds **M6** and **M7**, a second CT excitation ($S_0 \rightarrow S_2$) is present in the CT band (Fig. S2 (SI)). The $S_0 \rightarrow S_1$ and $S_0 \rightarrow S_2$ excitations correspond to HOMO → LUMO and HOMO → LUMO + 1 electronic transitions, both virtual orbitals being exclusively localized on the naphthalimide arms (see Fig. S2 for the pictograms of the LUMO + 1 orbitals of **M6** and **M7**). In the case of compound **M6**, the oscillator strength of $S_0 \rightarrow S_2$ transition is smaller as compared to $S_0 \rightarrow S_1$ (0.079 and 0.419 respectively). As for compound **M7**, the two CT electronic transitions, HOMO → LUMO and HOMO → LUMO + 1, are degenerate, (identical oscillator strengths values of 0.373). The increasing intensity of the charge transfer bands from **4** to **7** (Fig. 4 and S2 (SI)) is thus related to the presence of a second CT transition of increasing intensity in the order **M6** < **M7**.

The lowest energy absorption band of **5** is red shifted by ca. 20 nm in comparison with those of **4**, **6** and **7**. This effect is due to the electron donating ability of methoxy groups in the triphenylamino moiety of **5**, (see also the anti-bonding contribution of the methoxy groups in the shape of the HOMO orbital of **M5**, Fig. 2). By using the onset wavelengths of the absorption bands it was possible to roughly estimate the optical band gaps of the molecules which ranged from 2.40 to 2.58 eV (Table 3). The optical band gap of compound **5** containing methoxy groups in the *para* positions of

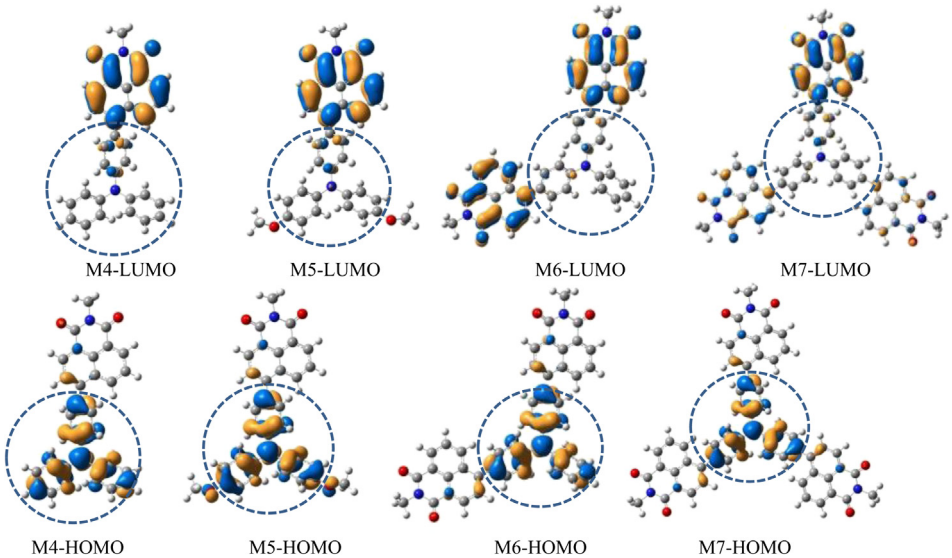

Fig. 2. Sketch of frontier orbitals for the model compounds M4–M7. The encircled parts delimit the TPA moiety. The frontier orbitals for the three molecules (Fig. 2) look very similar for all compounds, being localized almost entirely on the TPA core for the HOMO or naphthalimide moiety for the LUMO. The presence of the π-donor methoxy groups in **M5** is expected to destabilize the HOMO orbital [19] as compared to **M4**, which can also be deduced from the anti-bonding contribution of the methoxy groups in the shape of the HOMO orbital of **M5**.

Table 1
Thermal characteristics of compounds **4**–**7**.

Compound	T_g [°C] (2nd heating)	T_m [°C]	T_{ID} [°C]
4	47	134	437
5	45	–	429
6	76	136	448
7	84	141	483

T_m is melting point, T_g is glass transition temperature (both estimated by DSC), T_{ID} is 5% weight loss temperature estimated by TGA at a heating rate of 10 °C/min in N_2 atmosphere.

triphenylamino moiety is evaluated at 2.40 eV, which is by 0.15 eV lower than that of the corresponding derivative (**4**) containing no methoxy substituents (2.55 eV).

The absorption spectra of neat films of **4**–**7** and those of molecular dispersions in PS matrixes are presented in Fig. S1 (SI). The low energy absorption bands of the films are broader and slightly red shifted with respect to those of the dilute solutions. It is presumed that the red shifts of the absorption spectra of films as compared to those of solutions may be due to smaller dihedral angles in solid state, thus giving rise to more efficient π-conjugation and decreased HOMO-LUMO gap, but can also be due to more efficient π-stacking and stronger intermolecular interactions in the films than in dilute solutions [43]. Some degree of aggregation in the ground state may also be suspected to influence the absorption spectra of the films of these compounds. As a means to confirm this assumption, we have optimized dimers of different geometries for compounds **4** and **5** (Fig. 5).

The theoretical UV–VIS spectra corresponding to some of these dimers are presented in Figs. S3 and S4 (SI), showing the appearance of new transitions in the proximity of the HOMO → LUMO transition. Depending on the aggregation pattern, a blue or red shift of roughly 20–30 nm (0.12 eV) can be observed between the band maxima of dimer and monomer species (Figs. S3 and S4 (SI)), which seem to be due to the contribution of these new slightly higher energy transitions.

Fluorescence spectra of the dilute solutions of the synthesized compounds in nonpolar cyclohexane (10^{-6} mol L^{-1}), in polystyrene (PS) and of neat films are shown in Fig. 4. Fluorescence spectra of compounds **4, 6, 7** dissolved in nonpolar cyclohexane exhibit efficient molecular emission with fluorescence quantum yields of 0.63–0.78. The spectra show vibronic progression and pronounced Stokes-shift of ca. 55 nm. The Stokes-shift of compound **5** is of

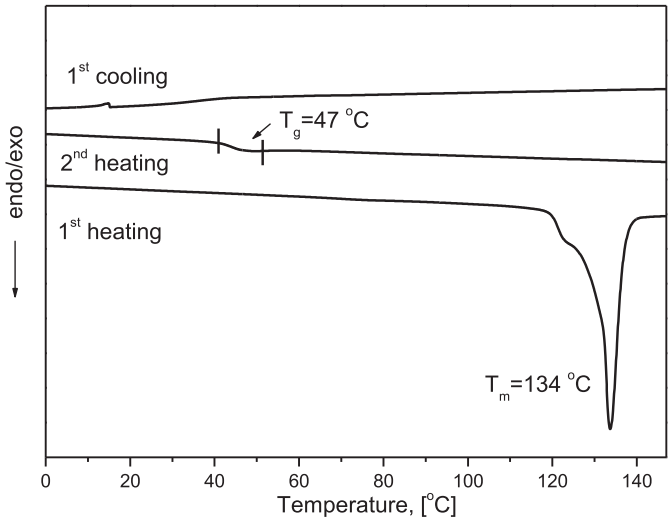

Fig. 3. DSC thermograms of compound **4** (scan rate of 10 °C/min, N_2 atmosphere).

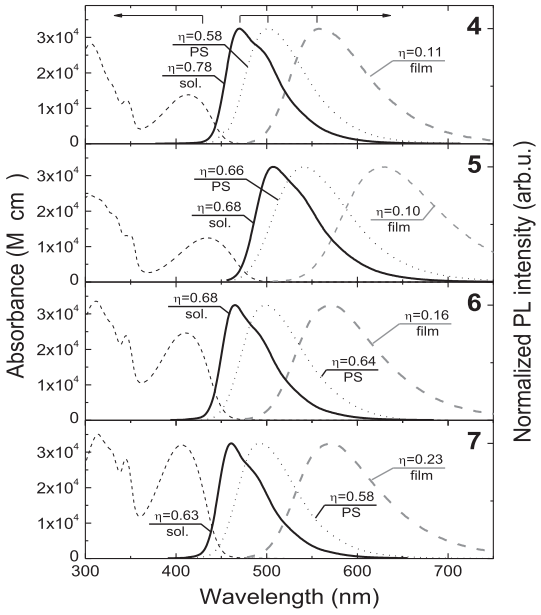

Fig. 4. Absorption (dashed thin line) and normalized fluorescence spectra of the 10^{-6} M solutions of compounds **4**–**7** in cyclohexane (thick, solid line), of neat films (dashed grey line) and of molecular dispersions in polystyrene matrix at 0.25 wt% concentration (dotted line). Fluorescence quantum yields are indicated.

72 nm. This observation indicates more polar nature of the excited states, but can also be due to the additional relaxations in the C–OMe bonds in compound **5** as compared to **4.** These bonds exhibit anti-bonding and non-bonding contributions at the HOMO and LUMO orbitals respectively (Fig. 2). After the HOMO → LUMO transition, the anti-bonding character vanishes, resulting in decreased C–O bond-lengths and non-negligible contribution in the relaxation energy (see also C–OMe bond-lengths in the neutral, cationic states, Fig. 1) [44]. The charge-transfer origin of the lowest transitions is revealed by the spectral properties of the compounds dissolved in solvents of various polarities. As it is evidenced in Fig. 6 the studied derivatives of TPA and 1,8-naphthalimide exhibit pronounced positive solvatochromic behaviour.

In the case of the solution of compound **5** in acetonitrile, the FL band is expected to be at about 850–950 nm and is undetectable.

Compound **4** is emitting at 470 nm in nonpolar cyclohexane and shows remarkable batochromatic shift of the fluorescence in THF (of 134 nm with respect to cyclohexane) and even larger red shift (of 258 nm with respect to cyclohexane) in acetonitrile. The fluorescence quantum yield of **4** is reduced down to 0.54 in THF and to 0.01 in acetonitrile. At the same time the absorbance spectra are only weakly shifted (by ca. 6 nm). Such solvatochromic behaviour is typical for compounds with significantly enhanced dipole moment in the excited state. Solvation effect is even more pronounced for compound **5** possessing polar methoxy groups in the donor triphenylamino moiety. The batochromatic shift of the fluorescence peak in THF solution is significantly larger (of 204 nm with respect to cyclohexane), while the fluorescence quantum yield is found to be below 0.01 (see Fig. 6(b)). The solvation-shift of fluorescence bands decreases with increase of the number of naphthalimide side arms, which is in line with reduced polarity of the excited state.

The dependence of the optical properties of the naphthalimide derivatives on the solvent polarity has been reported [45–48]. The fluorescence quenching in the most polar solvents was accounted for exciplex or cluster formation [45]. Solvatochromic behaviour of TPA and naphtahalimide derivatives seems to be different. It is very weak in absorbance, while it is much stronger in fluorescence. Such

Table 2
Photophysical characteristics of the dilute cyclohexane solutions, neat films and 0.25 wt% solid solutions in PS matrixes of compounds **4**–**7**.

Compound	Solution in cyclohexane							Neat film				In PS			
	λ_{abs}[a] (nm) (ε[b], L mol^{-1}cm^{-1})	λ_F^{max}[c] (nm)	η	τ (ns)	τ_R[d] (ns)	τ_{NR}[d] (ns)	λ_{teor}[e] (nm)	λ_{abs}[a] (nm)	λ_F^{max}[c] (nm)	η	τ_{avg} (ns)	λ_{abs}[a] (nm)	λ_F^{max}[c] (nm)	η	τ_{avg} (ns)
4	413 (13,821)	470	0.78	3.2	4.1	14.5	488	425	557	0.11	13.1	430	501	0.58	5
5	434 (12,459)	506	0.68	4.7	6.9	14.7	532	448	630	0.10	10.8	452	541	0.66	7.2
6	410 (24,658)	465	0.68	2.6	3.8	8.1	482	426	569	0.16	9.2	426	498	0.64	2.8
7	407 (32,025)	461	0.63	2.2	3.5	5.9	470	425	570	0.23	13.3	426	493	0.58	3.8

[a] Peak wavelength of absorption bands.
[b] Molar extinction coefficient.
[c] Wavelength at fluorescence band maximum.
[d] Radiative and non-radiative decay time constants calculated as τ/η and $\tau/(1-\eta)$, respectively.
[e] The theoretical $S_0 \rightarrow S_1$ values calculated at the TDB3LYP/6-31G(d,p) level.

behaviour is typical for the compounds with enhanced polarity in the excited state, what is in line with the DFT calculations [49].

The largest fluorescence quantum yield of 0.78 is found for the monosubstituted derivative of TPA (**4**) in nonpolar surrounding and it is steadily decreasing for compounds **6** and **7** down to 0.68 and 0.63, respectively. This is in contradiction with enhanced oscillator strength of the lowest transition of the compounds possessing one, two and three side arms (see Fig. 4) and thus less pronounced charge transfer character of the lowest excited states. Indeed, the radiative decay time systematically decreases in the order 3.2 ns, 2.6 ns and 2.2 ns for compounds **4**, **6**, **7**, respectively. However increase in the number of the singly bonded naphthalimide arms results in almost threefold increase in the rate of nonradiative recombination. Nonradiative decay time decreases in the order 14.5 ns, 8.1 ns and 5.6 ns for compounds **4**, **6**, **7**, respectively. Incorporation of the polar methoxy groups for compound **5** results in more expressed charge transfer character of the excited states and, thus enhanced excited state lifetime of 4.7 ns and decreased radiative decay rate with 6.9 ns radiative decay constant. Meanwhile the nonradiative decay constant is almost the same for both mono 1,8-naphthalimide-4-yl substituted compounds **4** and **5**.

Fluorescence spectra of the compounds molecularly dispersed in a rigid PS matrix are similar to those observed for the dilute solutions in nonpolar solvents. A systematic red shift of fluorescence spectra of about 20–30 nm is due to slightly different polarity of the media. Since in the case of solid dispersion the intramolecular motion is suppressed, few peculiarities of the emission are evident. Fluorescence spectra are broader and non-structured, the emission efficiency is slightly decreased and the fluorescence transients are non-exponential. This observation can be explained by "freezing" of the initial molecular geometry in the ground state [50,51]. However, the impact of restriction of intramolecular twisting is not strong. The largest decrease in fluorescence quantum yield (from 0.78 to 0.58) is observed for compound **4**.

Intramolecular interaction seems to have pronounced impact on the optical properties, particularly on emission properties of the solid films of compounds **4**–**7**. Fluorescence spectra are broad, unstructured and significantly red shifted. The Stokes shift is of 132 nm, 143 nm and 145 nm, and is weakly increasing with the number of naphthalimide arms, for compounds **4**, **6** and **7** respectively. It is strongly dependent on the polarity of the excited state and increases up to 182 nm for compound **5**, possessing polar methoxy groups. Such behaviour can be rationalized in the frame of the model of self-trapped excitons [52,53]. Non-exponential fluorescence decay and decreased fluorescence quantum yields indicate on the impact of exciton migration. Interestingly, the fluorescence quantum yield increases in the order 0.11, 0.16 and 0.23 for compounds **4**, **6** and **7**, respectively. This can be accounted for enhanced oscillator strength and reduced intramolecular vibrations.

3.5. Electrochemical and photoelectrical properties

In order to gain information on the charge injection capabilities, the electrochemical behaviour of compounds **4**–**7** were estimated by cyclic voltammetry at room temperature in dichloromethane solutions, using a three electrode system i.e. platinum rod as a counter electrode, glassy carbon as working electrode and Ag/$AgNO_3$ as the reference electrode. The measurements were carried out using 0.1 M tetrabutylammonium hexafluorophosphate ($TBAHFP_6$) as supporting electrolyte, scan rate 50 mV s^{-1}. Table 3 outlines the onset oxidation and reduction potentials of **4**–**7**. Fig. 7 shows cyclic voltammograms (CVs) of the compounds.

Compounds **4**–**7** displayed one reversible reduction peak, which might be due to the electron withdrawing nature of naphthalimide moieties, as well as one reversible oxidation peak, which might be attributed to the electron donating nature of TPA segment [54–56], suggesting that these compounds possess excellent electrochemical stability. The reduction current of **6** and **7** is obviously higher than that of the oxidation current in the cyclic voltammograms, suggesting that **6** and **7** can be classified as electron-accepting materials. The oxidative processes of **4**–**7** started at 0.54, 0.25, 0.57 and 0.58 V, respectively, and the reduction processes started at −1.83, −184, −1.84 and −1.80 V, respectively. The solid state ionization potentials (IP_{CV}) and electron affinities (EA_{SS}) were also estimated by using the empirical formulas $IP_{CV} = (E^{ox}_{onset} + 4.8)$ [eV] and $EA_{SS} = (E^{red}_{onset} + 4.8)$ [57] (Table 3).

In the anodic scan regime of the cyclic voltammogram of **5**, reversible oxidation peak at 0.49 V is observed which can be ascribed to oxidation of the electron-rich nitrogen atom in the TPA core. The irreversible oxidation peak at 1.14 V can be attributed to oxidation of methoxy groups, causing radical recombination and formation of a quinoid structure [58] and this observation is attributed to two-electron stepwise oxidation process.

An important characteristic of electronically active compounds intended for the application in optoelectronic devices is ionization potential (IP), which characterizes the electron releasing work under illumination. Except for the compound **5**, the IP_{CV} values deduced from the onset redox potentials range in a very small window (5.34–5.38 eV). The values of the ionization potentials (IP_{EP}) of the solid samples of compounds **4**–**7** were also estimated by electron photoemission spectrometry (Fig. 8) and the results are collected in Table 3.

The IP_{EP} of amorphous layers of the compounds **4**, **6**, and **7** range from 5.57 to 6.01 eV, indicating good air stability for these materials. Compounds **6** and **7** with two and three 1,8-naphthalimide moieties, respectively, demonstrated a little higher I_p values with respect to those of **4** and **5** with one 1,8-naphthalimide moiety.

Table 3
Electrochemical, photoelectrical, and theoretical electronic characteristics of **4**–**7**.

	E^{ox}_{onset} vs Fc/V[a]	E^{red}_{onset} vs Fc/V[a]	IP_{CV}, (eV)[b]	EA_{SS}, (eV)[b]	E^{opt}_{g} (eV)[c]	ε_{H}, (eV)[d]	ε_{L}, (eV)[d]	E_{I}, (eV)[e]
4	0.54	−1.83	5.34	−2.97	2.55	−5.28	−2.34	5.79 (6.39)
5	0.25	−1.84	5.05	−2.96	2.40	−4.96	−2.26	5.57 (5.97)
6	0.57	−1.84	5.37	−2.96	2.57	−5.48	−2.49	5.93 (6.45)
7	0.58	−1.80	5.38	−3.00	2.58	−5.68	−2.60	6.01 (6.51)

[a] E^{ox}_{onset} and E^{red}_{onset} are measured vs. ferrocene/ferrocenium.
[b] Calculated with reference to ferrocene (4.8 eV). Ionization potentials and electron affinities estimated according to $IP_{CV} = (E^{ox}_{onset} + 4.8)$ [eV]. $EA_{SS} = -(E^{red}_{onset} + 4.8)$ [eV] (where, E^{ox}_{onset} and E^{red}_{onset} are the onset reduction and oxidation potentials versus the Fc/Fc^{+}. E^{ox}_{onset} and E^{red}_{onset} of Fc/Fc+ measured in DCM solution containing 0.1 M $TBAHFP_6$ was 0.204 V vs. ferrocene/ferrocenium).
[c] The optical band gap estimated from the onset wavelength of optical absorption according to the formula: $E_g = 1240/\lambda_{edge}$, in which the λ_{edge} is the onset value of absorption spectrum in long wave direction.
[d] HOMO and LUMO energies corresponding to the isolated model compounds **M4**–**M7** calculated at the B3LYP/6-31G(d,p) level.
[e] Established from electron photoemission in air spectra. The values in parentheses correspond to the adiabatic IP of isolated model compounds **M4**–**M7**, calculated at the B3LYP/6-31G(d,p) level.

While the range of the electrochemical IP values is smaller than those estimated by the photoemission spectrometry, both methods provide similar trends, with the IP values for **5** being smaller by 0.2–0.3 eV as compared to **4**.

The trend in the theoretical IP values (Table 3) is in agreement with the experimental ones. In the frame of Koopmans' theorem (relating in this case the first I_p values to the HOMO energies) these trends can be explained by the similar evolution of the HOMO energies in these compounds (Table 3). The evolution in the HOMO energies in the order **4 > 6 > 7** is related to the electron withdrawing nature of 1,8-naphthalimide arms, whereas the small experimental and theoretical ranges of the IP values of compounds **4**, **6**, and **7** are due to the similar nature of their HOMO orbitals (Fig. 2). As for compound **5**, the higher HOMO energy (and smaller IP) as compared to that of **4** (by roughly 0.2–0.3 eV) is due to the strong π-donor effect of the methoxy groups, which can be observed in the anti-bonding contribution of this group in the HOMO orbital (Fig. 2).

3.6. Charge transport properties

Charge-transporting properties of the synthesized compounds were estimated by xerographic time-of-flight technique. Fig. 9 shows electric field dependencies of hole and electron drift mobilities for the molecular glasses of **4**–**7** and for the solid solution (50%) of compound **7** in bisphenol Z polycarbonate ((PC-Z), 1:1). Charge drift mobilities values are summarized in Table 4.

All the synthesized compounds are capable of transporting both holes and electrons. Their amorphous layers demonstrated hole drift mobility (μ_h) values reaching 10^{-7}–10^{-8} cm^2/V s at an electric field of 1×10^6 V/cm at room temperature and electron mobilities reaching 10^{-4}–10^{-5} cm^2/V s at the same electric field. Compound **5** showed the best ambipolar charge-transporting properties. Its amorphous layers showed the highest values of both hole and electron mobilities (Table 4). We did not manage to estimate electron mobilities in the layers of **7**. In order to confirm the ability of the compound to transport negative charge we estimated electron mobilities in the 50 wt% solid solutions of **7** in bisphenol Z. The dU/dt transients of electrons for the layer of **5** are shown in polycarbonate (PC-Z) and observed relatively high mobilities reaching 4.2×10^{-5} cm^2/V s at an electric field 1×10^6 V/cm (Fig. 10). It exhibited dispersive electron transport, which, along with the strong electric-field mobility dependence may suggest trap-dominant charge transport in this material. The electron transit times (t_t) needed for the estimation of electron mobilities were established from intersection points of two asymptotes from the double logarithmic plots. Dispersive charge transport was also observed for the other compounds studied in this work.

It is interesting to point out that, except for compound **5,** the electron mobilities are 2–3 orders of magnitude higher as compared to hole mobilities. Related to this observation, the ambipolar CT character of **5** is intriguing. Moreover, the larger hole mobility of compound **5** as compared to that of the parent compound **4** (by ~3 orders of magnitude) seems quite different form the results reported by Borsenberger et al. [59] and Maldonaldo et al. [17], in which, the lower hole mobilities for the substituted compounds had been related to the role of the increase (and the disorder) of the dipole moments induced by the substitutions. The calculated dipole moment for compounds **4** and **5** are 6.2 D and 6.5

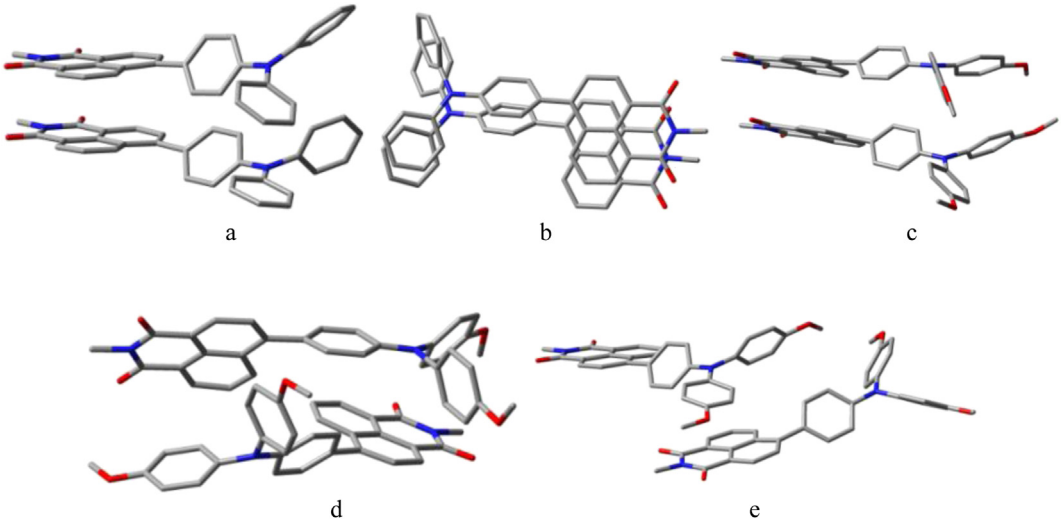

Fig. 5. Dimers of different geometries optimized at the wB97XD/6-31G(d,p) level: a) and b) two different views of the same dimer for compound **4**, reported here as Dim-M4-HH (head-to-head); c) dimer for compound **5**, reported here as Dim-M5-HH (head-to-head); d) dimer for compound **5**, reported here as Dim-M5-HT (head-to-tail); e) dimer for compound **5**, reported here as Dim-M5-DA (donor–acceptor).

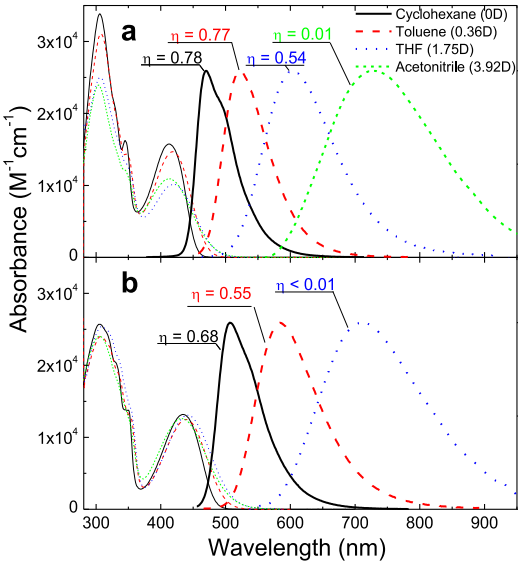

Fig. 6. Absorption and FL spectra of compounds **4** (a) and **5** (b) in dilute cyclohexane (black solid line), toluene (red dashed line), THF (blue dotted line), and acetonitrile (green short dashed line) solutions (10^{-6} M, $\lambda_{ex} = 450$ nm). (For interpretation of the references to colour in this figure legend, the reader is referred to the web version of this article.)

D respectively, which, in line with the results of Borsenberger et al. [59], suggests negligible role of this factor.

In order to obtain some more insight in these questions, we present a qualitative discussion of charge-transfer rate-constants (k_{CT}) based on the Marcus theory [20–23]. In the frame of Marcus' "hopping" mechanism, the rate-constant of a charge-transfer reaction between two adjacent molecules in amorphous materials can be calculated by means of the following equation:

$$k_{CT} = \frac{4\pi^2}{h}\frac{1}{\sqrt{4\pi\lambda k_B T}}t^2 \exp\left[\frac{-(\Delta G^\circ + \lambda)^2}{4k_B\lambda T}\right] \quad (1)$$

In this equation, t is the electronic coupling between two adjacent molecules, ΔG° is the free energy of the charge-transfer reaction (approximated to zero in the case of charge hopping between identical molecules in the absence of electric field), and λ is the reorganization energy. This last parameter is the sum of two terms: (i) λ_s, containing the contribution from the medium polarization energy. (ii) λ_i, representing the energetic effort due to the intra-molecular geometric relaxations related to the charge transfer between two adjacent molecules. In the following, some of these molecular parameters will be discussed, while the influence of morphological and other structural parameters will be ignored.

Based on equation (1), high charge-transfer rate-constants (k_{CT}) need minimal values of the reorganization energy (λ) and large values of the electronic coupling parameter (t). In order to compare compounds **4**–**7**, we have calculated some of these parameters and collected them in Table 5.

The hole reorganization energies (λ_i^h) of model compounds **M4**, **M6,** and **M7** are almost identical, which is due to the identical spatial distribution of the HOMO orbitals in these compounds (Fig. 2) The electron reorganization energies (λ_i^e) are also supposed to remain similar for **M4**, **M6**, and **M7** despite the increasing number of naphthalimide arms. Indeed, the coupling between the arms in **M7** (~0.023 eV) is much smaller than the reorganization energy of a single naphthalimide arm (0.399 eV for **M4**, Table 5), suggesting localization of the LUMO orbital in **M7** (and **M6**). Concerning the compound **M5**, both values are larger than for the other compounds. The much larger λ_i^h value for **M5** as compared to **M4** could be due to the additional contribution inherent to the relaxation of the C—OMe bonds. Indeed, the local anti-bonding contributions in the HOMO orbital at the C—OMe bonds (Fig. 2) are released in the cationic state, as indicated by the bond-length reduction of ~0.02 Å. As for λ_i^e, much smaller difference between **M5** and **M4** is found, which is mostly due to the space separation between the naphthalimide groups and the methoxy substituents in **M5**.

However, the main observation in Table 5 is that λ_i^e values are more important than the hole analogues, suggesting that this parameter cannot account for the larger electron mobilities found experimentally. Similarly, both λ_i^e and λ_i^h values for **M5** are larger than for the other compounds, which is in opposite agreement with the largest mobility values found for this compound. Consequently, in order to obtain better understanding of the experimental observations, we focus on the influence of the electronic coupling parameter (t). The calculation of the electronic couplings is based on the assumption that, despite the irregular packing between adjacent molecules in the amorphous materials, dimers of different geometries can be established. The t values calculated for two

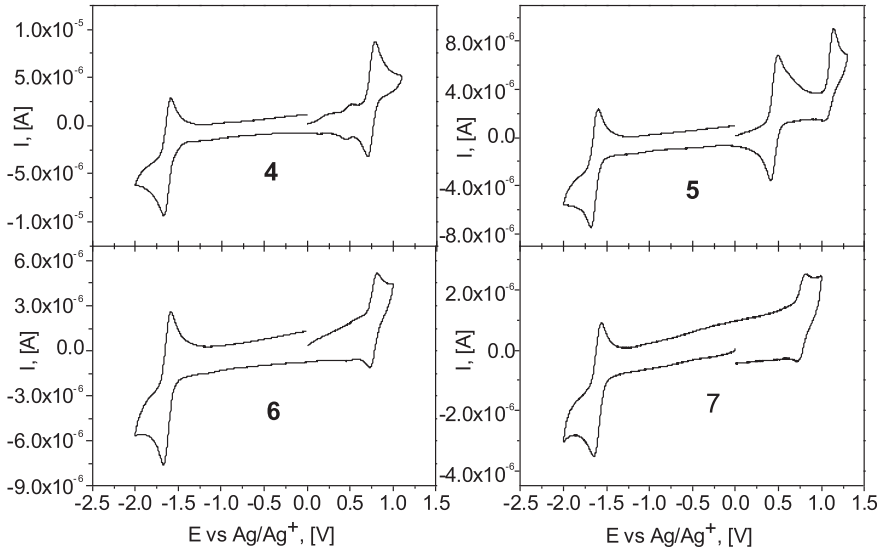

Fig. 7. Cyclic voltammograms of **4**–**7** (10^{-5} M solutions, scan rate of 50 mV s^{-1} vs Ag/Ag^+) in 0.1 M solution of $TBAHFP_6$ in CH_2Cl_2.

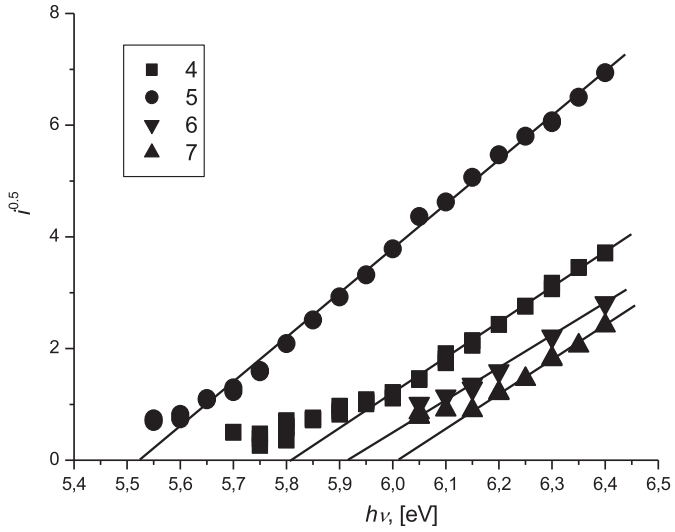

Fig. 8. Electron photoemission spectra of the neat layers of **4**–**7** recorded in air.

special dimers of compounds **4** and **5** (Dim-M4-HH and Dim-M4-HH, Fig. 5(a)–(c)), are given in Table 6 (lines 1–2).

In both cases, simultaneous donor-to-donor and acceptor-to-acceptor packing is assumed, which is similar to the packing reported in polymers containing naphthalimide and bi-thiophene alternated cores) [60]. The results given in Table 6 indicate larger *t* values for the holes, suggesting faster hole transfer, which, again, cannot account for the higher electron mobility found experimentally.

However, the static description provided so far considers only idealized dimer geometries, ignoring the displacements between molecules in the real materials. We suspect that this last factor may constitute a possible explanation for the above disagreements, as it has been pointed out in a recent similar study [61]. In order to give more insight in this respect, we firstly consider parallel displacements between adjacent molecules in the model dimer Dim-M4-HH shown in Fig. 5(b). A detailed analysis of the LUMO orbital of compound **4** (Fig. 2), indicates absence of nodal planes along the long axes, suggesting that the LUMO–LUMO overlap would be very little affected by small displacements between adjacent molecules in this direction. Similar analysis with respect to the HOMO orbital indicates the presence of nodes in the longitudinal direction,

Table 4
Hole and electron mobility data for the layers of compounds **4**–**7** and for the solid solution of **7** in PC-Z (50%).

Transport material, host polymer	Electron mobility μ_e, [cm^2/V s][a]	Hole mobility μ_h, [cm^2/V s][a]	α, [cm$^{1/2}$ V$^{-1/2}$]
Al+**4**	2.3×10^{-4}	3.7×10^{-7}	–
Al+**5**	7.5×10^{-4}	1.1×10^{-4}	0.013[c], 0.014[d]
Al+**6**	4.7×10^{-5}	4×10^{-7}	~0.0068[c], 0.0097[d]
Al+**7**	–	2×10^{-8}[b]	~0.008[d]
Al+[**7**+(PC-Z), 1:1]	4.2×10^{-5}	–	~0.0025[c]

[a] Hole and electron drift mobility values at electric field 1×10^6 V/cm.
[b] Hole drift mobility value at electric field 3.6×10^5 V/cm.
[c] Pool-Frenkel parameter for electrons.
[d] Pool-Frenkel parameter for holes.

suggesting much more sensitivity of the HOMO–HOMO overlap to the displacements in this direction. A similar conclusion has been reached also by Wetzelaer et al. [61] by calculating the LUMO–LUMO and HOMO–HOMO couplings for different reciprocal positions between molecules containing naphthalene diimide and bithiophene moieties. As for the transversal displacements (along the short axes of Dim-M4-HH), both HOMO and LUMO orbitals exhibit nodal surfaces, making the corresponding overlaps very sensitive to the displacements. However, the transversal displacements seem to be mostly limited by the steric hindrance between the long alkyl chains of naphthalimide groups on the one hand, and between the TPA phenyl groups on the other hand. One can thus suppose that, due to this kind of displacements, the overall variation in the orbital overlap should be larger for the HOMO orbitals. Larger disorder in the electronic couplings should be than expected for the hole transfer, which, in terms of disorder models [62] would result in smaller hole mobilities.

As for compound **5**, additional coupling schemes can be supposed, similar to those proposed previously [19]. Briefly, due to the presence of the methoxy groups, different types of C–H…π(Ph) or C–H…N,O hydrogen-bond interactions between TPA-OMe moieties of adjacent molecules have been assumed [19], resulting in strengthening of inter-molecular interactions. Stronger interactions between the TPA-OMe groups can be thus expected in the case of compound **5**, as suggested by the stronger dissociation energy found for Dim-M5-HH as compared to Dim-M4-HH (15.7 kcal mol^{-1} and 13.9 kcal mol^{-1}, Table 6). Consequently, in the case of Dim-M5-HH, reduced geometry disorder and reduced disorder in the HOMO–HOMO coupling would be expected as compared to Dim-M4-HH, resulting in enhanced hole mobility.

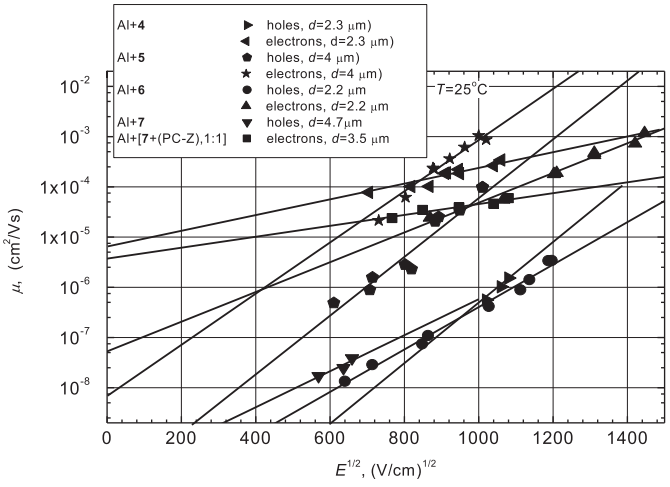

Fig. 9. Electric field dependencies of hole and electron drift mobilities for the layers of compounds **4**–**7**.

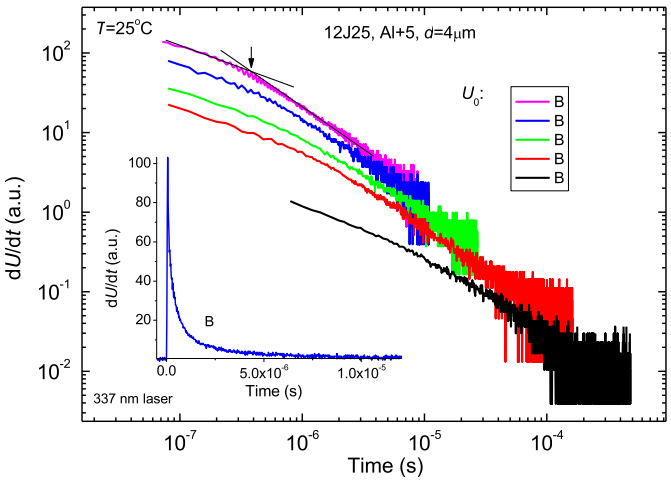

Fig. 10. XTOF transients of electrons for a neat film of **5**.

Table 5
Hole- and electron intramolecular reorganization energies for the model compounds **M4**–**M7** computed at the B3LYP/6-31G(d,p) level.

Compound	λ_i^h (eV)	λ_i^e (eV)
M4	0.139	0.399
M5	0.258	0.422
M6	0.138	[a]
M7	0.136	[a]

[a] Similar reorganization energy values as compared to **M4** can be assumed for **M6** and **M7**. See text for details.

Results for other dimer geometries, based on **M4** and **M5**, are also shown in Table 6. One can observe that the HOMO–HOMO couplings are generally larger for dimers containing no OMe groups, which seem to contradict the experimental trend of hole mobilities between **4** and **5**. However, systematically stronger interactions are found in the case of OMe-containing dimers, again suggesting that the disorder in HOMO–HOMO couplings should be strongly reduced for this compound as compared to **4**. Concluding this analysis, we suggest that the enhanced hole mobility and the ambipolar CT character of **5** result from the stronger interactions between adjacent molecules, making possible to maintain the hole transport rate at a comparable level as the electron one.

Admittedly, this semi-quantitative analysis can not provide thorough explanations, but aims only to point on some possible mechanisms allowing to better understand the difference between the hole and electron transport in these materials. Interestingly, packing patterns between naphthalimide moieties similar to those presented in Fig. 5(a)–(c) have been reported in polymers containing naphthalimide and bi-thiophene alternated cores [61] which comforts the validity of the above analysis.

Table 6
Electronic couplings (t) and dissociation energies (E_D, corrected for BSSE and ZPE) for some selected dimers of model compounds M4 and M5. The electronic couplings are calculated at the B3LYP/6-31G(d,p)/CPCM/wB97XD/6-31G(d,p) level. The dissociation energies are calculated at the CPCM/wB97XD/6-31G(d,p) level. Negative dissociation energies mean repulsive state (higher level calculations would slightly modify these values, however, the trends are expected to remain unchanged).

Model dimer		t^h (eV)	t^e (eV)	E_D (kcal mol^{-1})
Dim-M4-HH	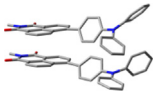	0.055	−0.032	13.9
Dim-M5-HH	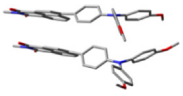	0.045	−0.027	15.7
Dim-M4-HT	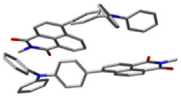	−0.007	0.052	8.5
Dim-M5-HT	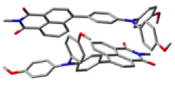	−0.028	−0.001	10.3
Dim-M4-DA	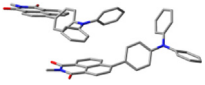	0.014	−0.001	3.4
Dim-M5-DA	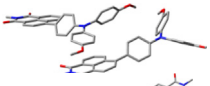	0.024	−0.004	3.9
Dim-M4-DD	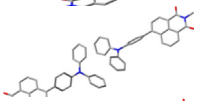	0.048	0.001	−1.9
Dim-M5-DD	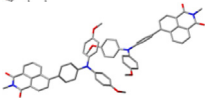	0.001	0.001	1.8

4. Conclusions

A series of ambipolar materials containing electron accepting 1,8-naphthalimide moieties and electron-donating triphenylamino groups were obtained via Suzuki cross-coupling reaction. The synthesized compounds exhibit high thermal stability. Their 5% weight loss temperatures range from 429 to 483 °C. All the synthesized compounds are capable of glass formation. Their glass transition temperatures are in the range from 45 to 84 °C. The dilute solutions of the compounds in nonpolar solvents and in rigid polystyrene solutions show fluorescence quantum yields from 0.58 to 0.78, while emission yields of the neat films are in the range of 0.10–0.23. Due to pronounced electron donor–acceptor character, in polar solvents the compounds show dramatic solvatochromic red shifts of fluorescence up to 250 nm, with significant reduction of the emission yield. Compound **5**, possessing polar methoxy groups in the donor triphenylamino moiety shows the strongest solvatochromic effect.

The ionization potentials of the layers of the synthesized compounds range from 5.57 to 6.01 eV. The lowest ionization potentials and the best charge-transporting properties were observed for the amorphous layers of 4-(4′-(di-(4″-methoxyphenyl)amino)phenyl)-*N*-(2-ethylhexyl)-1,8-naphthalimide (**5**). Electron mobilities of 7.5×10^{-4} cm^2 V^{-1} s^{-1} and hole mobilities of 1.1×10^{-4} cm^2 V^{-1} s^{-1} were recorded for this compound at an electric field of 1×10^6 V/cm. Compounds containing no methoxy groups exhibit electron mobilities by 2–3 order of magnitude higher than the hole mobilities. The comparison between compounds **4** and **5** shows that the methoxy groups increase the hole mobility by ~3 orders of magnitude. Theoretical results in the frame of hopping Marcus theory indicate that a static analysis, based on the comparison of the intramolecular reorganization energies and the electronic coupling parameter, predicts charge mobilities in opposite agreement with the experimental result. A semi-quantitative discussion of the positional disorder in some selected dimers from these molecules suggests that the larger electron mobility for the compounds containing no methoxy groups may be due to the smaller influence of the disorder between adjacent molecules on the LUMO–LUMO overlaps, as compared to the HOMO–HOMO overlaps. In the case of **5**, the presence of methoxy groups is shown to allow stronger interactions between adjacent molecules, making possible to maintain a good level of hole transfer for this compound. Finally, our results suggest that theoretical static analysis ignoring the effect of the disorder should be employed with precautions.

Acknowledgement

This research was funded by the European Social Fund under the **Global Grant** measure. Habil. Dr. V. Gaidelis from the Department of Solid State electronics, Vilnius University is thanked for the help in the measurements of ionization potentials. A. Sakalyte from the Department d'Enginyeria Química, Universitat Rovira i Virgili is thanked for the help in TGA measurements. The computer center of the University of Cergy-Pontoise, France is thanked for providing the computing resources. Dr. V. Coropceanu from Georgia Institute of Technology is thanked for stimulating discussions.

Appendix A. Supplementary data

Supplementary data related to this article can be found at http://dx.doi.org/10.1016/j.dyepig.2014.02.023.

References

[1] Shirota Y, Kageyama H. Charge carrier transporting molecular materials and their application in devices. Chem Rev 2007;107:953–1010.

[2] Kulkarni AP, Tonzola CJ, Babel A, Jenekhe SA. Electron transport materials for organic light-emitting diodes. Chem Mater 2004;16:4556–73.

[3] (a) Jung BJ, Tremblay NJ, Yeh ML, Katz HE. Molecular design and synthetic approaches to electron-transporting organic transistor semiconductors. Chem Mater 2011;23:568–582.
(b) Lei T, Dou JH, Cao XY, Wang JY, Pei J. A BDOPV-based donor–acceptor polymer for high-performance n-type and oxygen-doped ambipolar field-effect transistors. Adv Mater 2013;25:6589–6593.
(c) Lei T, Dou JH, Cao XY, Wang JY, Pei J. Electron-deficient poly(p-phenylene vinylene) provides electron mobility over 1 cm^2 $V^{(-1)}$ $s^{(-1)}$ under ambient conditions. J Am Chem Soc 2013;135:12168–71.

[4] (a) Duan LA, Qiao JA, Sun YD, Qiu Y. Strategies to design bipolar small molecules for OLEDs: donor–acceptor structure and non-donor–acceptor structure. Adv Mater 2011;23:1137–1144.
(b) Lei T, Jin-Hu Dou JH, Ma ZJ, Liu CJ, Wang JY, Pei J. Chlorination as a useful method to modulate conjugated polymers: balanced and ambient-stable ambipolar high-performance field-effect transistors and inverters based on chlorinated isoindigo polymers. Chem Sci 2013;4:2447–52.

[5] Chen Z, Lee MJ, Ashraf RS, Gu Y, Albert-Seifried S, Meedom Nielsen MM, et al. High performance ambipolar diketopyrrolopyrrole-thieno[3,2-b]thiophene copolymer field-effect transistors with balanced hole and electron mobilities. Adv Mater 2012;24:647–52.

[6] (a) Son KS, Yahiro M, Yoshizaki TIH, Adachi C. Analyzing bipolar carrier transport characteristics of diarylamino-substituted heterocyclic compounds in organic light-emitting diodes by probing electroluminescence spectra. Chem Mater 2008;20:4439–4446.
(b) Huang JH, Su JH, Li X, Lam MK, Fung KM, Fan HH, et al. Bipolar anthracene derivatives containing hole- and electron-transporting moieties for highly efficient blue electroluminescence devices. J Mater Chem 2011;21:2957–64.

[7] (a) Zheng CJ, Ye J, Lo MF, Fung MK, Ou XM, Zhang XH, et al. New ambipolar hosts based on carbazole and 4,5-diazafluorene units for highly efficient blue phosphorescent OLEDs with low efficiency roll-off. Chem Mater 2012;24:643–650.
(b) Qu SY, Hua JL, Tian H. New D-π-A dyes for efficient dye-sensitized solar cells. Sci Cina Ser B 2012;55:677–97.

[8] Castellanos S, Gaidelis V, Jankauskas V, Grazulevicius JV, Brillas E, Lopez-Calahorra F, et al. Stable radical cores: a key for bipolar charge transport in glass forming carbazole and indole derivatives. Chem Commun 2010;46:5130–2.

[9] Reghu RR, Bisoyi HK, Grazulevicius JV, Anjukandi P, Gaidelis V, Jankauskas V. Air stable electron-transporting and ambipolar bay substituted perylene bisimides. J Mater Chem 2011;21:7811–9.

[10] Liu YW, Niu FF, Lian JR, Zengk PJ, Niu HB. Synthesis and properties of starburst amorphous molecules: 1,3,5-tris(1,8-naphthalimide-4-yl)benzenes. Synth Met 2010;160:2055–60.

[11] (a) Iwan A, Sek D. Polymers with triphenylamine units: photonic and electroactive materials. Prog Polym Sci 2011;36:1277–325;
(b) Ning Z, Tian H. Triarylamine: a promising core unit for efficient photovoltaic materials. Chem Commun; 2009:5483–95;
(c) Jiang Y, Wang Y, Hua J, Tang J, Li B, Qian S, et al. Chem Commun 2010;46:4689–91.

[12] Pan JH, Chiu HL, Chen L, Wang BC. Theoretical investigations of triphenylamine derivatives as hole transporting materials in OLEDs: correlation of Hammett parameter of the substituent to ionization potential and reorganization energy level. Comput Mater Sci 2006;38:105–12.

[13] Takahashi S, Nozaki K, Kozaki M, Suzuki S, Keyaki K, Ichimura A, et al. Photoinduced electron transfer of *N*-[(3- and 4-diarylamino)phenyl]-1,8-naphthalimide dyads: orbital-orthogonal approach in a short-linked D-A system. J Phys Chem A 2008;112:2533–42.

[14] Gudeika D, Lygaitis R, Mimaitė V, Grazulevicius JV, Jankauskas V, Lapkowski M, et al. Hydrazones containing electron-accepting and electron-donating moieties. Dyes Pigments 2011;91:13–9.

[15] Seo ET, Nelson RF, Fritsch JM, Marcoux LS, Leedy DW, Adams RN. Anodic oxidation pathways of aromatic amines. Electrochemical and electron paramagnetic resonance studies. J Am Chem Soc 1966;88:3498–503.

[16] Pan JH, Chou YM, Chiu HL, Wang BC. Theoretical investigation of organic amines as hole transporting materials: correlation to the Hammett parameter of the substituent, ionization potential, and reorganization energy level. Aust J Chem 2009;62:483–92.

[17] Maldonado JL, Bishop M, Fuentes-Hernandez C, Caron P, Domercq B, Zhang YD, et al. Effect of substitution on the hole mobility of bis(diarylamino) biphenyl derivatives doped in poly(styrene). Chem Mater 2003;15:994–9.

[18] Hreha RD, George CP, Haldi A, Domercq B, Malagoli M, Barlow S, et al. 2,7-Bis(diarylamino)-9,9-dimethylfluorenes as hole-transport materials for organic light-emitting diodes. Adv Funct Mater 2003;13:967–73.

[19] Keruckas J, Lygaitis R, Simokaitiene J, Grazulevicius JV, Jankauskas V, Sini G. Influence of methoxy groups on the properties of 1,1-bis(4-aminophenyl) cyclohexane based arylamines: experimental and theoretical approach. J Mater Chem 2012;22:3015–27.

[20] Marcus RA. Electron transfer reactions in chemistry. Theory and experiment. Rev Mod Phys 1993;65:599–610.

[21] Levich VG. Present state of the theory of oxidation and reduction in solution (bulk and electrode reactions). Adv Electrochem Electrochem Eng 1966;4:249–71.

[22] Marcus RA. On the theory of oxidation–reduction reactions involving electron transfer I. J Chem Phys 1956;24:966–78.

[23] Marcus RA, Sutin N. Electron transfers in chemistry and biology. Biochim Biophys Acta 1985;811:265–322.

[24] Harwood LM, Moody CJ. Organic chemistry. Principles and practice. Blackwell Science; 1989.

[25] Chen BL, Zhang B, Cheng Y, Xie Z, Wang L, Jing X, et al. Pure and saturated red electroluminescent polyfl uorenes with dopant/host system and PLED efficiency/color purity trade-offs. Adv Funct Mater 2010;20:3143–53.

[26] Kim SW, Shim SC, Kim DY, Kim CY. Synthesis and properties of novel triphenylamine polymers containing ethynyl and aromatic moieties. Synth Met 2001;122:363–8.

[27] Nicolas M, Fabre B, Chapuzet JM, Lessard J, Simonet J. Boronic ester-substituted triphenylamines as new Lewis base-sensitive redox receptors. J Electroanal Chem 2000;482:211–6.

[28] Thelakkat M, Ostrauskaite J, Leopold A, Bausinger R, Haarer D. Fast and stable photorefractive systems with compatible photoconductors and bifunctional NLO-dyes. Chem Phys 2002;285:133–47.

[29] Miyamoto E, Yamaguchi Y, Yokoyama M. Ionization potential of organic pigment film by atmospheric photoelectron emission analysis. Electrophotography 1989;28:364–70.

[30] Kohn W, Sham L. Self-consistent equations including exchange and correlation effects. J Phys Rev 1965;140:A1133–8.

[31] (a) Lee CT, Yang WT, Parr RG. Development of the Colle-Salvetti correlation-energy formula into a functional of the electron density. Phys Rev B 1988;37:785–9;
(b) Becke AD. Density functional thermochemistry. III. The role of exact exchange. J Chem Phys 1993;98:5648–52.

[32] (a) Gross EKU, Kohn W. Local density-functional theory of frequency-dependent linear response. Phys Rev Lett 1985;55:2850–2;
(b) Runge E, Gross EKU. Density-functional theory for time-dependent systems. Phys Rev Lett 1984;52:997–1000;
(c) Gross EKU, Kohn W. Time-dependent density functional theory. Adv Quant Chem 1990;21:255–91;
(d) Bauernschmitt R, Ahlrichs R. Treatment of electronic excitations within the adiabatic approximation of time dependent density functional theory. Chem Phys Lett 1996;256:454–64;
(e) Casida ME, Jamorski C, Casida KC, Salahub DR. Molecular excitation energies to high-lying bound states from time-dependent density-functional response theory: characterization and correction of the time-dependent local density approximation ionization threshold. J Chem Phys 1998;108:4439–49.

[33] Bredas JL, Beljonne D, Coropceanu V, Cornil J. Charge-transfer and energy-transfer processes in π-conjugated oligomers and polymers: a molecular picture. Chem Rev 2004;104:4971–5004.

[34] Chai JD, Head-Gordon M. Long-range corrected hybrid density functionals with damped atom-atom dispersion corrections. Phys Chem Chem Phys 2008;10:6615–20.

[35] Sini G, Sears JS, Bredas JL. Evaluating the performance of DFT functionals in assessing the interaction energy and ground-state charge transfer of donor/acceptor complexes: tetrathiafulvalene–tetracyanoquinodimethane (TTF–TCNQ) as a model case. J Chem Theory Comput 2011;7:602–9.

[36] Steinmann NS, Pemontesi C, Delachat A, Corminboeuf C. Why are the interaction energies of charge-transfer complexes challenging for DFT? J Chem Theory Comput 2012;8:1629–40.

[37] (a) Barone V, Cossi M. Quantum calculation of molecular energies and energy gradients in solution by a conductor solvent model. J Phys Chem A 1998;102:1995–2001.
(b) Cossi M, Rega N, Scalmani G, Barone V. Energies, structures, and electronic properties of molecules in solution with the C-PCM solvation model. J Comput Chem 2003;24:669–81.

[38] Valeev EF, Coropceanu V, da Silva DA, Salman S, Bredas JL. Effect of electronic polarization on charge-transport parameters in molecular organic semiconductors. J Am Chem Soc 2006;128:9882–6.

[39] Frisch MJ, Trucks GW, Schlegel HB, Scuseria GE, Robb MA, Cheeseman JR, et al. Gaussian 09, revision B.01. Wallingford CT: Gaussian Inc.; 2010.

[40] Boys SF, Bernardi F. The calculation of small molecular interactions by the differences of separate total energies. Some procedures with reduced errors. Mol Phys 1970;19:553–66.

[41] Goodbrand HB, Hu NX. Ligand-accelerated catalysis of the ullmann condensation: application to hole conducting triarylamines. J Org Chem 1999;64:670–4.

[42] McMasters S, Kelly LA. Ground-state interactions of spermine-substituted naphthalimides with mononucleotides. J Phys Chem B 2006;110:1046–55.

[43] Tao S, Jiang Y, Lai SL, Fung MK, Zhou Y, Zhang X, et al. Efficient blue organic light-emitting devices with a new bipolar emitter. Org Electron 2011;12:358–63.
[44] After HOMO→LUMO transition, a somewhat zwitterionic structure is created, with positive charge in the TPA core and the negative one in the naphthalimide core. Calculations on the cationic and anionic compounds 4 and 5 confirm this assumption. The difference in the C-OMe bond-lengths between neutral and cationic state in 5 is roughly 0.02 Å (THF/B3LYP/6–31(d, p) level.
[45] Demets GJF, Triboni ER, Alvarez EB, Arantes GM, Filho PB, Politi MJ. Solvent influence on the photophysical properties of 4-methoxy-*N*-methyl-1,8-naphthalimide. Spectrochim Acta Part A 2006;63:220–6.
[46] Poteau X, Brown AI, Brown RG, Holmes C, Matthew D. Fluorescence switching in 4-amino-1,8-naphthalimides: "on–off–on" operation controlled by solvent and cations. Dyes Pigments 2000;47:91–105.
[47] Ramachandram B, Saroja G, Sankaran NB, Samanta A. Unusually high fluorescence enhancement of some 1,8-naphthalimide derivatives induced by transition metal salts. J Phys Chem B 2000;104:11824–32.
[48] Yuan D, Brown RG. Enhanced nonradiative decay in aqueous solutions of aminonaphthalimide derivatives via water-cluster formation. J Phys Chem A 1997;101:3461–6.
[49] The theoretical dipole moments in the ground state are 7.7D, 7.9D, 7.2D, and ~ 1D for compounds M4–M7 respectively (B3LYP/6-31G** level, in THF. The value of M7 does not correspond to the C3 geometry). Test single point calculations of M4 and M5 in the lowest triplet state (geometry of the singlet ground state, with the excited electron localized on the acceptor core) result in dipole moments of 24.5D and 29.8D respectively, thus giving a rough idea on the evolution of the dipole moments after charge separation in the excited state (we also remember that S1 is almost pure HOMO→LUMO transition).
[50] Krotkus S, Kazlauskas K, Miasojedovas A, Gruodis A, Tomkeviciene A, Grazulevicius JV, et al. Pyrenyl-functionalized fluorene and carbazole derivatives as blue light emitters. J Phys Chem C 2012;116:7561–72.
[51] Gulbinas V, Kodis G, Jursenas S, Valkunas L, Gruodis A, Mialocq JC, et al. Charge transfer induced excited state twisting of *n,n*-dimethylaminobenzylidene-1,3-indandione in solution. J Phys Chem A 1999;103(20):3969–80.
[52] Harrer D, Pilpott MR. In: Agranivich VM, Hochstrasser RM, editors. Spectroscopy and excitation dynamics of condensed molecular systems. Amsterdam: North Holland; 1983. p. 27.
[53] Jursenas S, Gruodis A, Kodis G, Chachisvilis M, Gulbinas V, Silinsh EA, et al. Free and self-trapped charge-transfer excitons in crystals of dipolar molecules of *n,n*-dimethylaminobenzylidene 1,3-indandione. J Phys Chem B 1998;102:1086–94.
[54] Segura JL, Gómez R, Blanco R, Reinold E, Bäuerle P. Synthesis and electronic properties of anthraquinone-, tetracyanoanthraquinodimethane-, and perylenetetracarboxylic diimide-functionalized poly(3,4-ethylenedioxythiophenes). Chem Mater 2006;18:2834–47.
[55] Segura JL, Gómez R, Reinold E, Bäuerle P. Synthesis and electropolymerization of a perylenebisimide-functionalized 3,4-ethylenedioxythiophene (EDOT) derivative. Org Lett 2005;7:2345–8.
[56] Gómez R, Veldman D, Blanco R, Seoane C, Segura JL, Janssen RAJ. Energy and electron transfer in a poly(fluorene-*alt*-phenylene) bearing perylenediimides as pendant electron acceptor groups. Macromolecules 2007;40:2760–72.
[57] Jones BA, Facchetti A, Wasielewski MR, Marks TJ. Tuning orbital energetics in arylene diimide semiconductors. Materials design for ambient stability of n-type charge transport. J Am Chem Soc 2007;129:15259–78.
[58] Hsiao SH, Liou GYS, Kung YC, Hsiung TJ. Synthesis and properties of new aromatic polyamides with redox-active 2,4-dimethoxytriphenylamine moieties. J Polym Sci Polym Chem 2010;48:3392–401.
[59] Borsenberger PM, Magin EH, O'Regan MB, Sinicropi JA. The role of dipole-moments on the hole transport in triphenylamine-doped polymers. J Pol Sci 1996;34:317–23.
[60] Rivnay J, Toney MF, Zheng Y, Kauvar IV, Chen Z, Wagner V, et al. Unconventional face-on texture and exceptional in-plane order of a high mobility n-type polymer. Adv Mater 2010;22:4359–63.
[61] Wetzelaer Gert-Jan AH, Kuik M, Olivier Y, Lemaur V, Cornil J, Fabiano S, et al. Asymmetric electron and hole transport in a high-mobility *n*-type conjugated polymer. Phys Rev B 2012;86:165203–11.
[62] Bassler H. Charge transport in disordered organic photoconductors a monte carlo simulation study. Phys Status Solidi B 1993;175:15–56.